FEA based Transformer Loss Analysis for Dual Active Bridge DC-DC Converter using Triple Phase Shift Modulation

Seema Mir Akbar[1,2], Ammar Hasan[1], Alan J. Watson[2](Senior Member, IEEE) and Pat Wheeler[2] (Fellow, IEEE)
[1]School of Electrical Engineering and Computer Science, National University of Sciences and Technology, Pakistan
[2]Power Electronics Machines and Control Group, University of Nottingham, Nottingham NG7 2RD, U.K.
Corresponding author: seema.akbar@nottingham.ac.uk

Abstract—**High frequency transformers are a key component of dual active bridge (DAB) dc-dc converters, providing isolation and voltage scaling. The losses in the transformer should be minimized to improve efficiency and extend lifetime. The existing research focuses on the optimization of design parameters, such as core material, cross sectional area and winding configuration to minimize losses. However, the transformer losses also depend on the harmonic content of the current as well as the design parameters and thus the efficiency can be further improved by selecting a modulation scheme which results in minimum current harmonics. This paper evaluates the effect of modulation schemes on the transformer losses of a DAB converter operating under triple phase shift (TPS) modulation by using finite element analysis. A comparison of losses under different modes of TPS modulation has been provided and it is proved that losses can be significantly reduced by selecting optimal modulation schemes. The experimental results performed on a 1kW DAB converter laboratory prototype are provided to validate the proposed work. Moreover, a generalized framework has been proposed to analyze and optimize transformer losses for isolated converters.**

Index Terms—**Dual active bridge (DAB) dc-dc converter, finite element analysis (FEA), triple phase shift (TPS), winding loss.**

I. Introduction

In recent years, isolated bidirectional dual active bridge (DAB) dc-dc converters, first proposed in [1] have gained popularity in the research community. DAB dc-dc converters are capable of bidirectional power flow, galvanic isolation, and have the potential for high power density and soft switching realization. As a result, it is considered, in various forms for use in high voltage DC transmission (HVDC), power quality improvement devices, renewable energy sources, flexible AC transmission system (FACTS) and drives systems [2]–[5].

The DAB dc-dc converter, shown in Fig.1, consists of two H-bridges (HB) galvanically isolated by a high frequency transformer. The transformer provides galvanic isolation between the two HBs, and can also step up/down voltage. Furthermore, the leakage inductance of the transformer is used to support the control of power flow through the converter. The average transmission power and the output voltage level of the converter can be controlled by modulating the phase shift ratios of the two HBs. Various modulation techniques have been proposed in the literature, and can be categorized as single phase shift (SPS)[6], extended phase shift (EPS)[6], dual phase shift (DPS) and triple phase shift (TPS) [7].

In DAB dc-dc converters nearly 20 percent of the total losses are consumed in the form of transformer and inductor losses while around 35 percent of the total losses are in the form of switching loss[8]. The rest is a result of conduction and auxiliary losses [8]. Thus, switching losses are a major source of loss in the DAB converter which cannot be ignored in any situation. The main focus of current research is to consider the modulation schemes that result in soft switching, in order to minimize the switching losses, and also to reduce the switch current stress to minimize conduction losses. Compared to other modulation schemes, TPS utilizes all three available phase shift ratios of the converter. Based on the ranges of the three phase shift ratios, many distinct modes of operation can be obtained Each mode offers a different peak current and waveform, suggesting a different harmonic content for the same output voltage and transmission power with more than one mode that satisfy soft switching [7], [9]. The focus of the TPS modulation schemes is to reduce the current stress, eliminate reactive power in the high frequency ac link and extend the soft switching operating range to improve the efficiency and the life expectancy of the semiconductor devices[6]-[7],[9]–[12]. However, the transformer losses, which play a significant role in the overall efficiency of the converter, and the impact of different modulation schemes on the transformer losses are not discussed in the existing literature.

High frequency transformers can consume significant

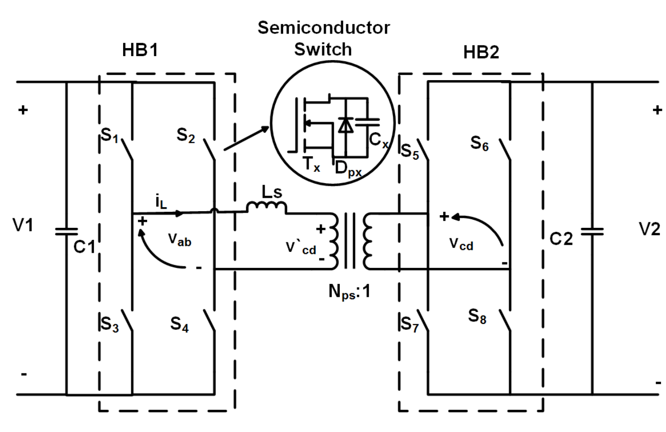

Fig. 1. Isolated Bidirectional DAB dc-dc converter

amount of power in the form of winding and core losses [13]. The winding power loss, which is typically 60-80% of the total loss of the transformer is significantly influenced by the high frequency eddy currents that cause skin and proximity effects [12], [13]. The transformer used in a DAB dc-dc converter is subject to non-sinusoidal waveforms containing high frequency harmonic content which increases the winding power loss. The temperature of the transformer rises as a result of this high power loss. Consequently, hot spots can be induced on the surface of transformer, which can damage the insulation of the winding, resulting in local burnouts. Moreover, the rise in temperature reduces the operational transformer ratings. Therefore, transformer losses need to be minimized for the efficient operation of the DAB dc-dc converter and it is important that the harmonic content and peak value of the ac current should be taken into consideration to achieve maximum efficiency. However, the existing research effort appears to be working towards optimization of the design parameters of the transformer such as core material, size of core and number of windings in order to minimize the transformer losses and increase the power density [14]–[26]. An optimization approach based on the brute force technique has been used in [19], which evaluates different combinations of design parameters to obtain maximum efficiency and power density. Similarly, a grid based optimization technique has been used to find the optimal design parameter in [20]. Machine learning based approaches have been used in [21] and [22] to obtain the optimal design parameters. Scaling laws to optimize medium frequency transformer have been suggested in [23]. An air core transformer has been presented in [24] to reduce the complexity, cost and size of the converter. Another approach to reduce the overall size of the transformer has been presented in [25] by integrating the required inductance of the converter in the transformer.

The aforementioned literature has not included any insight into to the reduction of the transformer losses during operation. [27] provides design procedure of an AC-DC DAB converter for optimizing efficiency and power density. A comparison of transformer efficiency has been provided in [28] for multilevel Si and SiC DAB converters and it is shown that 3 level modulation is an optimized modulation scheme for high power density, high efficiency and low cost. A modulation based on the analytical expressions has been suggested in [29] with focus to minimize losses and extend ZVS in AC-DC DAB converter. An optimized modulation scheme is also provided for DPS in [30] by including the transformer losses in the optimization function. However, different modes available under TPS and its effect on the transformer losses due to the unique harmonic content have not been evaluated in any of the discussed literature. The aim of this research is to analyze the impact of the modulation schemes specifically for TPS modulations scheme on the power loss of the transformer with given design parameters.

To evaluate the effect of modulation schemes, the resultant currents generated by the five different operating modes of TPS modulation defined in [7] as unified TPS (UTPS) have been selected in this research; UTPS is a current stress optimized scheme that presents closed form solutions for the phase shift ratios for each of the five defined modes[7]. The power losses of the transformer in a DAB dc-dc converter are calculated in steady state using finite element analysis (FEA)[31],[32] performed using ANSYS Maxwell for each of the five operating modes. This research shows that the winding power loss is distinct for each mode even though some modes have the same peak currents. Moreover, it is also presented in this research that core loss is also different for each mode due to the non-identical shape of waveforms. The operating mode which results in minimum transformer loss for a specific power range is presented based on this analysis. A comparison between the modes with minimum and maximum transformer losses is provided which shows that approximately, 3-5% of the total power can be saved by selecting the optimal modulation scheme. Furthermore, a generalized framework based on the methodology used in this research to calculate the transformer losses in any isolated converter is presented. A hardware prototype with the same parameters as the ANSYS Maxwell simulation has been constructed in the lab and experiments have been performed to verify the presented scheme.

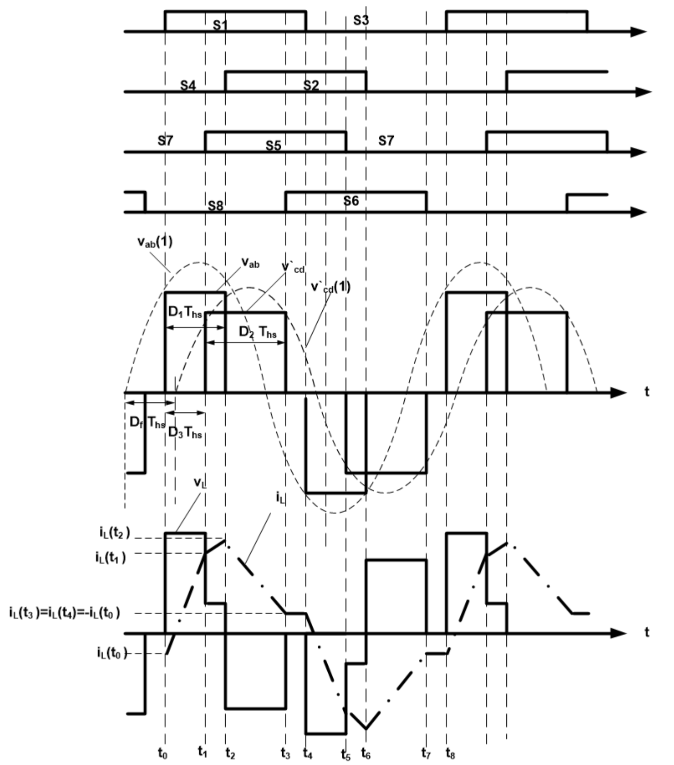

Fig. 2. General operating waveforms of DAB with TPS modulation

The remaining parts of the paper are organized as follows. Section-II provides a detailed discussion on UTPS and the optimized values of phase shift ratios. Section-III provides a detailed analysis of the power losses occurring in the transformer. Moreover, this section also includes a comparative analysis of various techniques to calculate losses. Section-IV discusses the finite element method (FEM) used to calculate the transformer losses and the analysis of these losses for each mode of UTPS performed in ANSYS. The details of the laboratory prototype of DAB dc-dc converter and experimental results are presented in section-V. Section-VI discusses the overall efficiency of the converter. Section-VII presents the generalized methodology which can be used to optimize the transformer losses in isolated converters. Section-VIII concludes the paper.

II. Unified Triple Phase Shift

A DAB dc-dc converter is shown in Fig.1, along with its general operating waveforms under TPS control in Fig.2. V_1 and V_2 are the dc voltages of the two HBs of the converter, v_{ab} and v'_{cd} are the ac equivalent voltages of HBs on V_1 side. v'_{cd} is given by the product of N_{ps} and v_{ab}, where N_{ps} denotes the primary to secondary turns ratio of the transformer. The semiconductor switch is denoted by S_x, which consists of the active switch T_x, anti-parallel diode D_{px}, and the junction capacitance, denoted by C_x. L_s is the sum of series inductance and leakage inductance of the transformer and i_L is the inductor current. T_s is the switching period while T_{hs} is half switching period. The inner phase shift ratios for HB1 and HB2 are defined as D_1 with range $0 \leq D_1 \leq 1$ and D_2 with range $0 \leq D_2 \leq 1$, respectively, while D_3 with range $-1 \leq D_3 \leq 1$ is the outer phase shift ratio between v_{ab} and v'_{cd}. Moreover, D_f is defined as the phase shift ratio between the fundamental components of v_{ab} and v'_{cd} , which is related to other phase shift ratios given by:

$$D_f = D_3 + D_2/2 - D_1/2 \tag{1}$$

Expressions for base values of power P_b and current I_b, defined in terms of input voltage V_1, series inductance L_s and switching period T_s are given by Eq: 2

$$I_b = \frac{V_1 T_s}{2\pi L_s},\ P_b = \frac{V_1^2 T_s}{2\pi L_s} \tag{2}$$

The required transmission power is represented by P_o and P_{on} will be used to represent the value of required transmission power normalized to the base power P_b. I_{pn} will represent current stress normalized to the base current I_b.

The switches on the same leg of the DAB always conduct in alternate half cycles such as S_1 and S_3 as shown in Fig.2, similarly S_2 and S_4 also conduct in alternate half cycles. The phase shift ratio between the turning on of switch S_1 and S_2 is D_1, as shown in Fig. 2. Switches S_1 and S_4 are on and conducting in this duration while S_2 and S_3 are not conducting resulting in voltage V_{ab} across the output of HB1, which is equal to V_{in}. S_2 is turned on at the end of D_1 interval, thus S_1 and S_2 are conducting during this interval with zero voltage created across the output terminals of the HB1. This state continues until switch S_1 is turned off at the end of the half cycle. From the start of the next half cycle, S_2 and S_3 conduct until S_2 is switched off. The magnitude of V_{ab} is same as the input voltage but with negative direction during this interval.

Similarly, on the second bridge, HB2, D_2 is the phase shift ratio between the turning on of switch S_5 and S_6. As shown in Fig.2, switches S_5 and S_8 conduct for this duration while S_6 and S_7 are turned off, thus V_{cd} is equal to V_0. S_6 is turned on after D_2, therefore S_5 and S_6 are conducting during this interval forcing zero voltage until switch S_5 is turned off. S_6 and S_7 start conducting at the end of the half cycle until S_6 is turned off. The magnitude of V_{cd} is equal to the output voltage with negative direction.

TABLE I
MODE OPERATIONAL CONSTRAINTS [7]

Switching Mode	Mode operational constraints
Mode I	$0 \leq D_f \leq \frac{D_2}{2} - \frac{D_1}{2}$
Mode II	$0 \leq D_f \leq \frac{D_1}{2} - \frac{D_2}{2}$
Mode III	$\left\lvert \frac{D_1}{2} - \frac{D_2}{2} \right\rvert \leq D_f \leq min(\frac{D_1}{2} + \frac{D_2}{2}, 1 - \frac{D_1}{2} - \frac{D_2}{2})$
Mode IV	$1 - \frac{D_1}{2} - \frac{D_2}{2} \leq D_f \leq \frac{D_1}{2} + \frac{D_2}{2}$
Mode V	$\frac{D_1}{2} + \frac{D_2}{2} \leq D_f \leq 1 - \frac{D_1}{2} - \frac{D_2}{2}$

D_3 is the phase shift ratio between the first switch S_1 of first bridge and the first switch S_5 of the second bridge, which is same as the phase shift ratio between the voltages V_{ab} and $\grave{V}_{cd}$. The slope of the inductor current varies based on the switching pattern as shown in the Fig. 2, and a switching period can be divided into small intervals depending on the shape of current waveform.

Five distinct switching modes are obtained based on the switching sequence of the two HBs. The operating waveform for all modes, which are used to derive the expression of normalized transmission power and current stress are presented in [7]. The main contribution of UTPS is to derive optimal control parameters to minimize current stress with the required transmission power and voltage conversion ratio d, where the control parameters are the optimal values of the three phase shift ratios (D_f, D_1, D_2). Thus, the optimization approach aims to find optimal values of phase shift ratios ($D_{f,opt}$, $D_{1,opt}$, $D_{2,opt}$) from the specified mode determined by the operational constraints presented in Table I, which minimize current stress I_{pn} at the required transmission power P_{on} and conversion ratio, d, where $d < 1$.

A Karush-Kuhn-Tucker (KKT) approach, which takes into account all of the equality and inequality constraints in solving the optimization problem, has been used to find the optimized solution given by X^*=($D_{f,opt}$, $D_{1,opt}$, $D_{2,opt}$) for minimum current stress. The boundary conditions of the optimal phase shifts result in two different transmission power ranges, the lower transmission power range is identified as range-A and the higher transmission power range is referred as range-B . The optimal phase shift ratios resulting in minimum current and the transmission power ranges arising from the optimal control parameters of each mode are given in the Table II.

III. Transformer Losses

A. Types of Losses

Transformer structures consist mainly of a core, made of electromagnetic material, and the windings, usually made of copper. Thus there are two types of losses: core loss, and winding loss.

1) Core Loss: The core loss is composed of the hysteresis loss, eddy current loss and the residual loss [33]. The

TABLE II
OPTIMAL CONTROL PARAMETERS FOR SELECTED SWITCHING MODES[7]

Mode	Power range	Local optimal control parameters
Mode I	IA: $[0, \frac{(1-d)d^2\pi}{2}]$	$D_{1,opt} = \sqrt{\frac{2P_{on}}{(1-d)\pi}},\ \frac{D_{1,opt}}{d} \leq D_{2,opt} \leq 1,\ D_{fopt} = \frac{\sqrt{2(1-d)\pi P_{on}}}{2d\pi}$
	IB: $[\frac{(1-d)d^2\pi}{2}, \frac{d\pi}{8}]$	$D_{1,opt} = \begin{cases} \frac{1}{2} - \frac{1}{2}\sqrt{\frac{d\pi-8P_{on}}{d\pi}}, 0 < d \leq \frac{1}{2} \\ \frac{1}{2} + \frac{1}{2}\sqrt{\frac{d\pi-8P_{on}}{d\pi}}, \frac{1}{2} < d \leq 0 \end{cases},\ D_{2,opt} = 1,\ D_{f,opt} = \begin{cases} \frac{1}{4} - \frac{1}{4}\sqrt{\frac{d\pi-8P_{on}}{d\pi}}, 0 < d \leq \frac{1}{2} \\ \frac{1}{4} + \frac{1}{4}\sqrt{\frac{d\pi-8P_{on}}{d\pi}}, \frac{1}{2} < d \leq 0 \end{cases}$
Mode II	IIA: $[0, \frac{d(1-d)\pi}{2(2-d)^2}]$	$D_{1,opt} = (2-d)\sqrt{\frac{2P_{on}}{d(1-d)\pi}},\ D_{2,opt} = \sqrt{\frac{2P_{on}}{d(1-d)\pi}},\ D_{f,opt} = \frac{\sqrt{2(1-d)\pi P_{on}}}{2d\pi}$
	IIB: $[\frac{d(1-d)\pi}{2(2-d)^2}, \frac{d\pi}{8}]$	$D_{1,opt} = 1,\ D_{2,opt} = \frac{1}{2} + \frac{1}{2}\sqrt{\frac{d\pi-8P_{on}}{d\pi}},\ D_{f,opt} = \frac{1}{4} + \frac{1}{4}\sqrt{\frac{d\pi-8P_{on}}{d\pi}},$
Mode III	IIIA: $[0, \frac{(1-d)d^2\pi}{2}]$	$D_{1,opt} = \sqrt{\frac{2P_{on}}{(1-d)\pi}},\ D_{2,opt} = \frac{1}{d}\sqrt{\frac{2P_{on}}{d(1-d)\pi}},\ D_{fopt} = \frac{\sqrt{2(1-d)\pi P_{on}}}{2d\pi}$
	IIIB: $[\frac{(1-d)d^2\pi}{2}, \frac{d\pi}{6}]$	$D_{1,opt} = \frac{2}{3} - \frac{1}{3}\sqrt{\frac{(2-3d)^2(d\pi-6P_{on})}{(1-3d+3d^2)d\pi}},\ D_{2,opt} = \frac{2}{3} - \frac{1}{3(2-3d)}\sqrt{\frac{(2-3d)^2(d\pi-6P_{on})}{(1-3d+3d^2)d\pi}}$ $D_{f,opt} = \frac{1}{3} - \frac{1-3d}{6(2-3d)}\sqrt{\frac{(2-3d)^2(d\pi-6P_{on})}{(1-3d+3d^2)d\pi}},$
Mode IV	IVA: $[0, \frac{(1-d)d^2\pi}{2}]$	$D_{1,opt} = \begin{cases} \frac{1}{2} - \frac{1}{2}\sqrt{\frac{d\pi-8P_{on}}{d\pi}}, 0 < d \leq \frac{1}{2} \\ \frac{1}{2} + \frac{1}{2}\sqrt{\frac{d\pi-8P_{on}}{d\pi}}, \frac{1}{2} < d \leq 0 \end{cases},\ D_{2,opt} = 1,\ D_{f,opt} = \begin{cases} \frac{1}{4} - \frac{1}{4}\sqrt{\frac{d\pi-8P_{on}}{d\pi}}, 0 < d \leq \frac{1}{2} \\ \frac{1}{4} + \frac{1}{4}\sqrt{\frac{d\pi-8P_{on}}{d\pi}}, \frac{1}{2} < d \leq 0 \end{cases}$
	IVB: $[\frac{(1-d)d^2\pi}{2}, \frac{d\pi}{4}]$	$D_{1,opt} = 1-(1-d)\sqrt{\frac{d\pi-4P_{on}}{(1-2d+2d^2)d\pi}},\ D_{2,opt} = 1,\ D_{f,opt} = \frac{1}{2} - \frac{1}{2}\sqrt{\frac{d(d\pi-4P_{on})}{(1-2d+2d^2)\pi}}$
Mode V	VA: $[0, \frac{d^2\pi}{2(1+d)^2}]$	$D_{1,opt} = \frac{\sqrt{2\pi P_{on}}}{\pi},\ D_{2,opt} = \frac{\sqrt{2\pi P_{on}}}{d\pi},\ D_{f,opt} = \frac{(1+d)\sqrt{2\pi P_{on}}}{2d\pi}$
	VB: $[\frac{d^2\pi}{2(1+d)^2}, \frac{d\pi}{8}]$	$D_{1,opt} = \frac{1}{2} - \frac{1}{2}\sqrt{\frac{d\pi-8P_{on}}{d\pi}},\ D_{2,opt} = \frac{1}{2} + \frac{1}{2}\sqrt{\frac{d\pi-8P_{on}}{d\pi}},\ D_{f,opt} = \frac{1}{2}$

hysteresis loss is the power lost during the magnetization and demagnetization of the core, caused by the multi-valued nature of the B-H curve. Thus, it is dependent on the frequency of the magnetizing force, f, and the area of the hysteresis loop, which in turn depends on the square of magnetic flux density [34],[35].

The eddy current loss is caused by the current flowing in the core due to a time varying magnetic field. Its generating mechanism is similar to the current flowing in the conductor, and has the same effects as the ohmic loss. Eddy current loss is directly proportional to the square of frequency, f, and the square of magnetic flux density, B [36].

The residual loss is due to the relaxation processes and occurs when the magnetic material has to establish a new equilibrium position during changes in thermal equilibrium. It is a small fraction of the loss as compared to hysteresis and eddy current loss and is directly proportional to the frequency, f, and magnetic flux density, B [33].

2) Winding Loss: The winding loss, also commonly known as copper loss, depends on the frequency, the structure of the conductors and the relative geometric position of the conductors to other conductors as well as to the magnetic core of the transformer. It consists of the ohmic part or loss due to dc resistance and an ac part due to ac resistance[37],[38].

The two effects that increase the ac resistance are: skin effect and proximity effect. Under high frequency operational conditions, the concentration of current increases near the surface of the conductor due to skin effect. Skin depth is a measure of the distance at which the current penetrates into the conductor, it is given by [39]:

$$\delta = \frac{1}{\sqrt{\pi f \sigma \mu_0 \mu_r}} \tag{3}$$

where δ is the skin depth, σ is the conductivity of the conductor, and μ_0 and μ_{r} is absolute and relative permeability of the conductor, respectively. Therefore, skin depth decreases with an increase in frequency as shown in Eq. (3). Hence, the effective area of the conductor is reduced as the current tends to flow only in the circumference of the conductor and not in the whole conductor area.

Proximity effect is the eddy current effect caused by the alternating magnetic field of one conductor on another conductor in its vicinity. This causes the current to concentrate on one side of the conductor, which is in the close proximity of another current carrying conductor. Thus, the effective area for ac current flow decreases, which in turn increases the resistance. This resistance further increases at a higher frequency, which causes the winding loss to increase [40].

B. Calculation of transformer losses

Several techniques have been proposed in the literature to calculate core loss [41]–[48] and winding loss [49]–[52]. Core loss calculation methods can be categorized into two groups: loss separation and empirical methods. In the loss separation method, core loss is divided into three components- hysteresis loss, eddy current loss and residual loss. However, this method requires extensive experimentation and curve fitting techniques to calculate the coefficients and consider all components of the loss, which makes its application potentially impractical.

The original Steinmetz equation (OSE), presented by Steinmetz, is an empirical formula, which is widely used to calculate the core loss [42]. It is given by:

$$P_{core} = K f^{\alpha} B_m^{\beta} \tag{4}$$

where P_{core} is the core loss, f is the fundamental frequency and B_{m} is the maximum flux density of the magnetizing force. Furthermore, K, α and β are the constants, which depend on the material of the core, that can be determined by manufacturers data sheet or by curve fitting techniques. The OSE has good accuracy for sinusoidal excitation. However, it is not suitable for the transformers used in all power electronics converters due to the non sinusoidal excitation of the component. Several adjustments to the OSE such as the modified Steinmetz equation (MSE) [44], generalized Steinmetz equation(GSE) [45] and the improved generalized Steinmetz equation (iGSE) [46] have been suggested to enhance the performance of OSE. However, all these calculations are based on the arbitrary waveforms. Moreover, comparative experimental results show poor correlation [41],[47], [48].

Winding loss has a significant effect on the efficiency of the DAB dc-dc converter and has gained the attention of researchers working on these converter types. Many analytical formulas have been derived to calculate winding loss, the most popular one is Dowell equation presented in [50]. It is based on one-dimensional (1-D) Maxwell equation, the analytical expression to calculate the AC resistance factor (F_R) derived by Dowell. This is given by:

$$F_R = \Delta \frac{\sinh 2\Delta + \sin 2\Delta}{\cosh 2\Delta - \cos 2\Delta} + \frac{2(m^2-1)\Delta}{3} \frac{\sin h\Delta + \sin \Delta}{\cosh \Delta - \cos \Delta} \quad (5)$$

where Δ is the normalized foil thickness with reference to the skin depth δ, and m is the number of layers of each winding portion. Dowell has assumed parallel inter layered magnetic field to the symmetry axis of the magnetic component. However, its physical validity has been questioned by many researchers [53], [54]. Although a correction factor named as the porosity factor has been suggested to rectify the Dowell equation [55], [56], it is time consuming to create a model and solve it for a specific device while the formula derived is limited to a specific part of the winding [32].

Ferreira has presented a closed form expression by considering the exact solution of the magnetic field of a round conductor by taking into account the skin and proximity effects [51]. However, the porosity factor is not suggested, resulting in an inaccurate evaluation of AC resistance factor [52]. Moreover, many other analytical expressions have been presented in [57]–[60].

Analytical techniques are good to analyze magnetic components, however, these approaches consider 1-D magnetic field distribution and thus ignore many other phenomena which greatly contribute to the losses in transformer. First, analytical techniques neglect the orthogonal magnetic fields assuming constant field intensity at each conductor layer[61],[62]. Second, windings are assumed to be part of an infinite sheet with constant current density along the surface of each layer, thus ignoring the edge effect [61]. Third important factor is the power loss due to the fringing effect in the air gap. Usually gapped ferrite cores are used to design inductors, the introduction of the air gap causes fringing magnetic field at the air gap resulting in excess power loss in the copper windings. The lines of leaked magnetic flux counteract the useful current by inducing the eddy currents thus reducing the effective area of the conductor and increasing the ac resistance as well as the power loss[63], [64].

Recently, the finite element method has gained significant attention for modelling various nonlinear electromagnetic materials with sinusoidal or other forms of excitation. Since FEA tools can analyze such field distributions, their application provide a better alternative to analytical methods [61]–[64]. The FEM has been used to calculate transformer parameters as well as losses [63]–[65]. Moreover, FEM is usually used as a benchmark to prove the validity of the novel analytical equations to analyze the magnetic losses [65], [66], therefore FEM has been used in this research to analyze and calculate the accurate transformer losses. Many powerful software programs, such as ANSYS, COMSOL and FEMLAB have been developed for the calculation of different types of transformer losses and other transformer parameters such as leakage inductance and winding resistance.

A 2D or 3D FEM model is constructed, based on the real transformer dimensions and geometry. Transient electromagnetic field analysis is then used to calculate the losses in the transformer, which involves spatial and temporal discretization of the physical equations.

The FEM solves a set of Maxwell equations [66]–[69] in order to calculate the losses of the transformer for a given excitation and frequency. Domain decomposition along a time-axis is used to perform transient analysis to solve all time steps simultaneously. Properties of the material, as well as boundary conditions can be defined for the transformer model. Material properties are characterized by a B-H curve. Transient FEM analysis then calculates core and the winding loss of the transformer for a specific frequency.

IV. Analysis and Proposed Scheme to Minimize Transformer Losses

As discussed in section-II, five modes arise in TPS modulation with a unique maximum value of current and a distinct waveform shape. This section discusses the FEM setup in ANSYS [70] to calculate the transformer losses for each mode of operation. It provides the analysis of the obtained results and proves that transformer losses not only depend on the magnitude of current but also on the harmonic content of the current. Hence, each mode will result in different operational losses.

A. FEM setup

ANSYS Maxwell 2D has been used to evaluate the transformer losses. The magnetic part of the DAB dc-dc converter which consists of the transformer and an additional inductor has been designed in ANSYS Maxwell as shown in Fig. 3. The transformer has been designed with axial symmetry RZ as shown in Fig. 4. An E59/31/22 core from EPCOS is used. The material of the core is N97, which is suitable for medium frequency. Concentric windings are used on the central leg of the rectangular core transformer. The turns ratio of the transformer is 1:1 with 20 turns on each winding. Similarly, the inductor has also been designed in ANSYS using an E59/31/22 core.

The average power losses at steady state for each mode must be calculated. Therefore, the transient solution setup

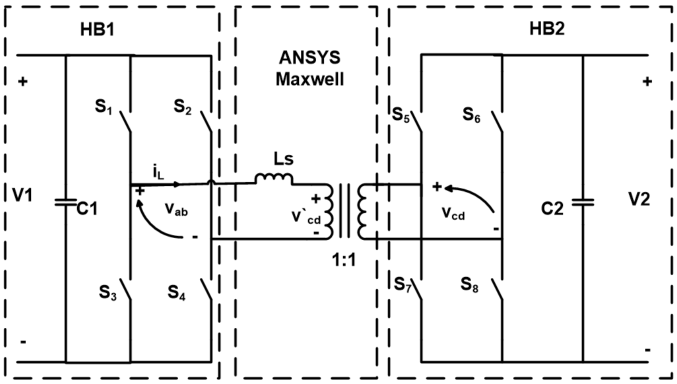

Fig. 3. Parts of DAB dc-dc converter built in ANSYS Maxwell

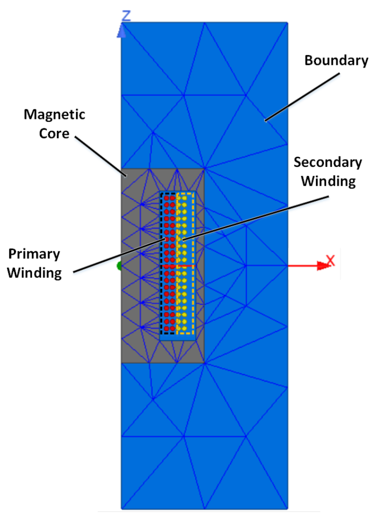

Fig. 4. Transformer model in ANSYS Maxwell with mesh

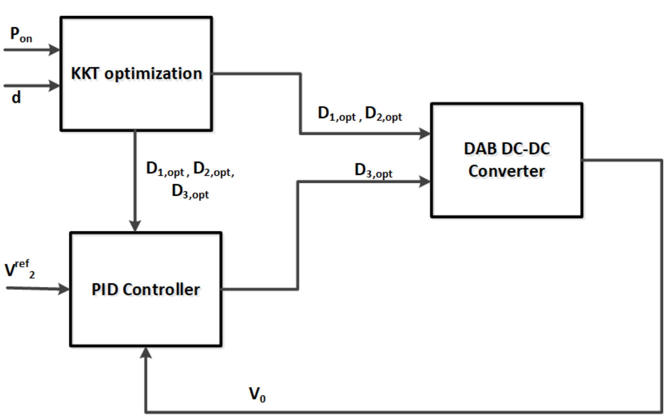

Fig. 5. Block diagram showing the operation of DAB converter

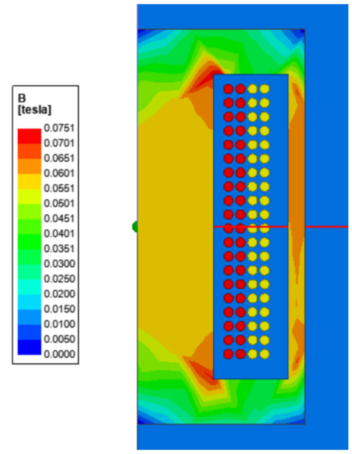

Fig. 6. Field distribution in transformer generated by current waveforms obtained from DAB dc-dc converter operating at P_o=241 watts, Input Voltage $V_1 = 230V$, Output Voltage $V_2^{ref} = 138V$, Conversion ratio d=0.6 and switching frequency f=20kHz.

TABLE III
PARAMETERS OF DAB DC-DC CONVERTER USED IN SIMULATIONS

Parameters	Values
Input voltage V_1	230V
Reference output voltage $V^{ref}{}_2$	138V
Conversion ratio d	0.6
Input Capacitance C_p	480 μF
Output Capacitance C_s	150 μF
Inductance value L_s	226.6 μH
Design of Transformer core	ETD 59/31/22
Material of transformer core	N97
Number of turns	20:20
Transformer ratio	1:1
Switching frequency	20 kHz

is used. The transient solution setup performs the FEA for one specific frequency for a specified time interval in contrast to other solution setups available in ANSYS Maxwell, which examines frequency response by analyzing converter at different frequencies. The power ferrite core loss model is used to calculate the core losses. The B-H curve obtained from the data sheet of the N-97 has been used to calculate the coefficients of the core loss model.

The transformer and series inductor windings are excited with the ac current generated from a DAB dc-dc converter using data from a PLECS[71] simulation as well as with data

TABLE IV
PER UNIT TRANSMISSION POWER RANGES FOR d=0.6

Mode	Minimum power	Maximum power
Mode-IA	0	0.22608
Mode-IB	0.22608	0.2355
Mode-IIA	0	0.19922
Mode-IIB	0.19922	0.2355
Mode-IIIA	0	0.22608
Mode-IIIB	0.22608	0.314
Mode-IVA	0	0.22608
Mode-IVB	0.22608	0.471
Mode-VA	0	0.22078
Mode-VB	0.22078	0.2355

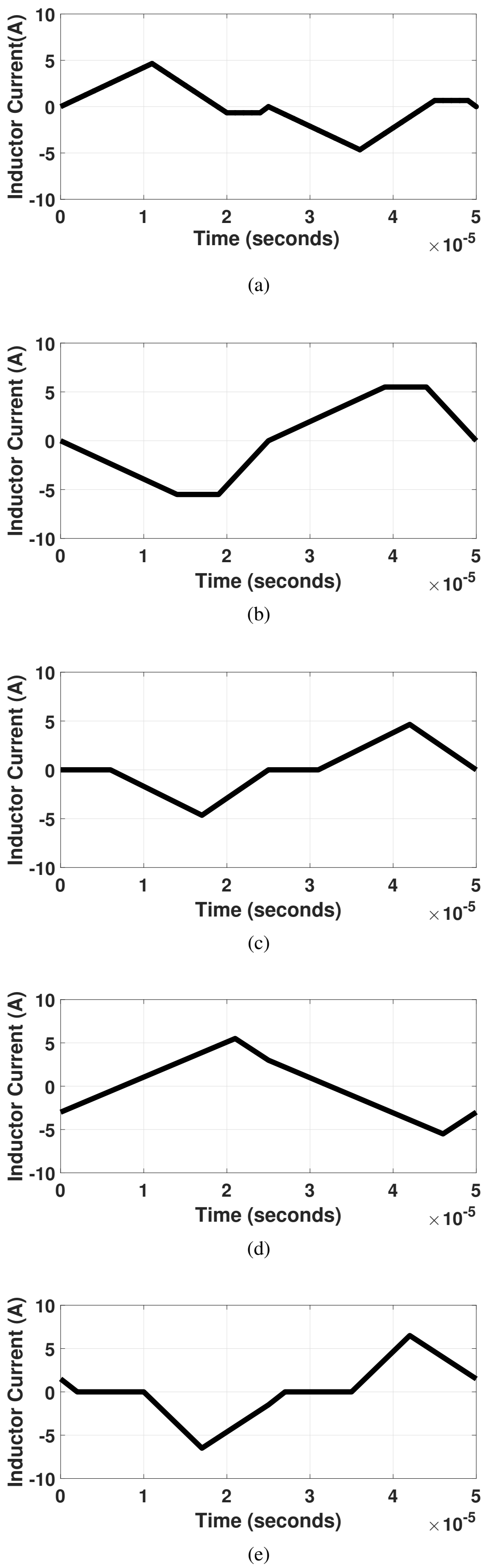

Fig. 7. Inductor current for P_o=241 watts, Input Voltage $V_1 = 230V$, Output Voltage $V_2^{ref} = 138V$, Conversion ratio d=0.6 and switching frequency f=20kHz. (a) Mode-1 (b) Mode-2 (c) Mode-3 (d) Mode-4 (e) Mode-5

from the experimental setup as discussed later in the article. Primary and secondary winding are excited separately from the primary and secondary currents, respectively, whereas the magnetizing current is the difference of the primary and secondary currents.

The parameters of DAB dc-dc converter are given in Table III. Fixed values of $D_{1,opt}$ and $D_{2,opt}$ are used, which are found from the UTPS calculations. Proportional, integral and differential (PID) control is used to regulate the output voltage by adjusting $D_{3,opt}$, whereas the initial value of $D_{3,opt}$ is calculated from the UTPS theory. The operation of the converter is shown in Fig. 5.

The processing time required to conduct the FEA at one power setting for a specific time duration depends on the system model internal dynamics as well as mesh length and time step. Mesh length plays an important role, as there is a trade-off between the accuracy of the results and the time taken by the analysis. Accuracy of results increases by selecting a small mesh length, but the time to conduct FEA significantly increases. As a result, an optimal mesh length should be selected for better performance considering a reasonable processing time. In this work, a length of 5mm is assigned to the mesh. The transformer structure with the mesh is shown in Fig. 4. The time step selection is another crucial parameter, which also affects performance and processing time. Since the converter is operated at a switching frequency of 20kHz, which results in a waveform with a time period of 50μs, the time step should be small enough to precisely sample the generated waveform in the converter simulation. Therefore, for this work, a minimum time step of 0.25μs and a maximum time step of 2μs have been selected.

B. Analysis of the results and optimal modes of operation

The field distribution in the transformer and the current waveforms for each operating mode of UTPS for d=0.6 and P_o=241 watts, which lies in the range of transmission power range-A, are shown in Fig. 6 and Fig. 7, respectively. Transmission power ranges for d=0.6 are given in Table IV; ranges of transmission power depends on the value of conversion ratios for a constant value of input voltage and series inductance. The maximum achievable per unit value of transmission power is $\frac{d}{4\pi}$, which is same as the maximum transmission power of SPS modulation and can only be obtained using the mode-IV modulation scheme. Each waveform has a different shape and as a result there is a different harmonic content in each case. The resultant winding loss, core loss and total losses in the transformer as well as current stress and data from frequency analysis for each mode are given in Table V. The lowest amount of winding loss occurs in mode-3, although mode-1 and mode-3 have the same current stress and peak current at the fundamental frequency. However, mode-1 has a higher total harmonic distortion (THD) than mode-3, thus the winding loss increases in mode-1. Therefore, it is clear that the winding loss of the transformer not only depends upon the current stress but also on the harmonic content of the current flowing through the transformer winding. Moreover, a comparison of the results for mode-2 and mode-5 shows that although the current stress of mode-5 is greater than mode-2, the loss in mode-5 is less than mode-2 due to the lower fundamental frequency component of mode-5. A further inference can be obtained by analyzing mode-4 and mode-5. The fundamental component of current in mode-4 is greater than the fundamental component of current in mode-5. However, mode-5 results in high losses because it has a higher THD than mode-4.

The transformer losses for each mode with different transmission power setting have been calculated while keeping the voltage ratio and other parameters constant for comparison purposes. The same procedure has been repeated for different values voltage ratio upto $d = 0.95$. Winding loss, core loss and total losses are plotted against transmission power P_o as shown in Fig.8, Fig.9 and Fig.10, respectively. Although the same results were obtained for different voltage ratios the authors have included only one setting of the voltage ratio for brevity. Fig. 8(a) presents the winding loss for different transmission power P_o in range-A for each of the five modes in steady state operation of the DAB dc-dc converter. The minimum winding loss occurs in mode-3 if the transmission power is in range-A. However, mode-3 does not provide optimal control parameters if the transmission power is high i.e, it lies in range-B. The optimal control parameters can be obtained using mode-4, achieving the minimum winding loss as evident from Fig. 8(b).

The resultant core loss for each mode is shown in Fig. 9. This figure shows that the core loss is very low when compared to the winding loss. The total losses of the transformer, which are the sum of core and winding loss are shown in Fig.10. It shows that the minimum losses occur in mode-3 in the lower transmission range while mode-4 results in the minimum losses for the higher transmission range. Therefore, transformer efficiency can be improved by only minimizing the winding loss. Fig. 11 provides a comparison of the minimum and maximum amount of losses occurring in the transformer. This presents the minimum losses that occurs in mode-3 and mode-4 for low and high power ranges, respectively, and the maximum power losses that occurs in mode-2 and mode-5. This comparison shows that losses can be significantly minimized by carefully selecting the mode of operation.

The proposed optimal modulation scheme based on the results obtained from this research study, with the previously described setup and parameters, can be summarized in the flow chart in Fig. 12. Base values for the transmission power and current stress are calculated using the series inductance L_s, switching frequency f_s and input voltage V_1 as given in Eq. 2. The next step is to check for the range of transmission power. If the transmission power is in the range 0 to $\frac{(1-d)d^2\pi}{2}$ then mode-3 should be used to calculate the optimal control parameters to achieve minimum losses in the transformer. Otherwise the control parameters calculated using mode-4 should be used since they result in minimum losses at higher transmission power. It can also be inferred from Fig. 11 that 3-5% of the total power can be saved by using the presented scheme.

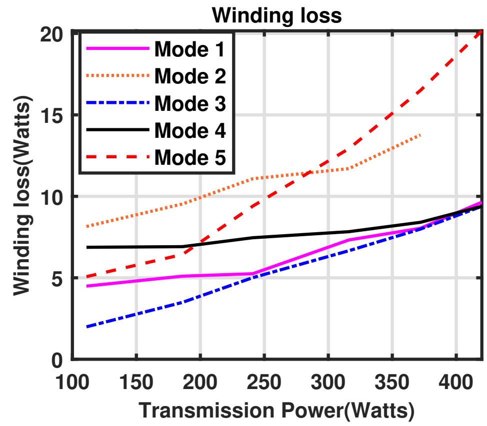

(a)

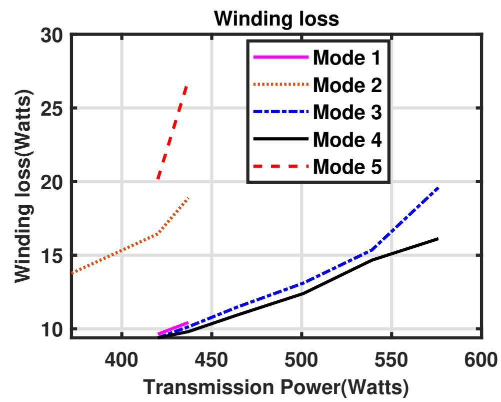

(b)

Fig. 8. Winding Losses of transformer in isolated bidirectional DAB converter with Input Voltage $V_1 = 230V$, Output Voltage $V_2^{ref} = 138V$, Conversion ratio d=0.6 and switching frequency f=20kHz.. (a) Power transmission range-A. (b) Power transmission range-B

V. Experimental Results

The proposed work has been validated by performing experiments on a 1kW laboratory prototype. The experimental prototype is shown in Fig. 13. The main components used in the design of the hardware are listed in Table VI. The series inductance consists of the leakage inductance of the transformer and an external inductor. IGBTs are used as switching devices to form the HBs. A TMS320F2837xD evaluation board from Texas Instruments, which communicates with a host computer, has been used as the digital control platform.

The transformer losses for each mode of UTPS modulation with different transmission power settings have been calculated while keeping the voltage ratio and other control parameters constant. The input voltage is maintained at 230 V and supplied from a DC source (SM300-10D). A DC electronic load is used to obtain different values of resistance at the output while regulating the output voltage to 138V. $D_{1,opt}$, $D_{2,opt}$ and $D_{3,opt}$ are calculated from the UTPS modulation equations given in Table II [7]. A PID control has been implemented to regulate the output voltage at 138V by adjusting D_3. The total losses of the transformer, formed from the sum of core and winding losses are calculated by measuring the transformer input and output power when the converter achieves steady

TABLE V
HARMONIC ANALYSIS OF INDUCTOR CURRENT OF ALL MODES FOR P_O=241 WATTS,SWITCHING FREQUENCY F=20KHZ, CONVERSION RATIO $d = 0.6$ WITH INPUT VOLTAGE $V_1 = 230V$ AND OUTPUT VOLTAGE $V_2^{ref} = 138V$

Mode	Mode 1	Mode 2	Mode 3	Mode 4	Mode 5
Winding losses (W)	5.25	11.08	4.97	7.2549	9.4
Core losses (W)	0.301	0.473	0.256	0.306	0.651
Total losses (W)	5.5317	11.553	5.226	7.5609	10.051
Current Stress (A)	4.651	5.50	4.651	5.50	6
Fundamental component (A)	3.106	5.24	3.12	4.28	4.072
3rd Harmonic	37.08%	14.74%	33.14 %	13.73%	41.25%
5th Harmonic	2.60 %	3.92 %	6.13%	5.83%	7.35%
7th Harmonic	6.20%	1.92%	3.56 %	3.06 %	3.62%
9th Harmonic	1.36 %	0.63%	2.36%	1.65%	3.23%
Total Harmonic Distortion	37.96 %	15.49%	34.14 %	13.73 %	42.30%

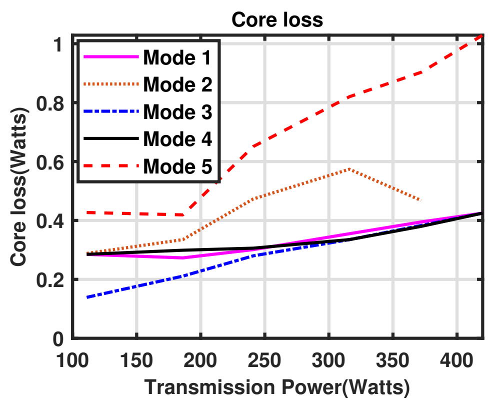

(a)

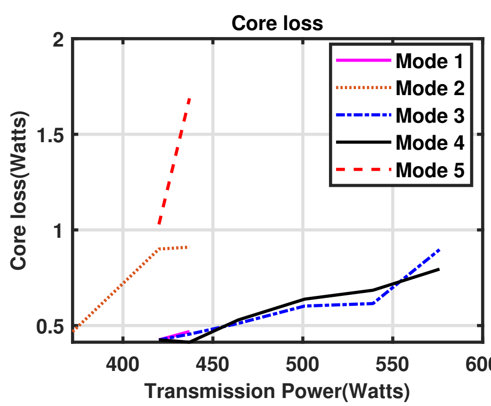

(b)

Fig. 9. Core Loss of transformer in isolated bidirectional DAB converter Input Voltage $V_1 = 230V$, Output Voltage $V_2^{ref} = 138V$, Conversion ratio d=0.6.(a) Power transmission range-A. (b) Power transmission range-B

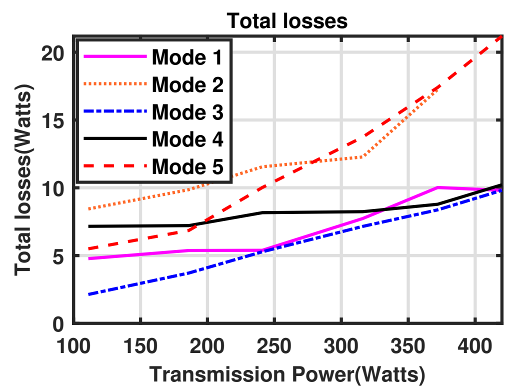

(a)

(b)

Fig. 10. Total Losses of transformer in isolated bidirectional DAB converter with Input Voltage $V_1 = 230V$, Output Voltage $V_2^{ref} = 138V$, Conversion ratio d=0.6 and switching frequency f=20kHz..(a) Power transmission range-A. (b) Power transmission range-B

state. The transformer losses are calculated for each mode using a different transmission power setting. The total losses are plotted against the transmission power for each mode. Current probes and an oscilloscope have been used to record the input and output current of the transformer, which is then used to carry out the analysis presented in the previous section.

Transformer losses in range-A for each mode are shown in Fig.14(a). The experimental data show that when the transmission power P_{on} is in range-A,then the minimum transformer losses occur when the converter is operating under mode-3, while mode-2 and mode-5 result in the highest losses. Hence, this data validates the hypothesis presented, based on the FEA carried out to analyze the effect of harmonics on transformer losses.

Fig. 14b presents the total losses of the transformer for all modes when the transmission power P_{on} is in range-B. It shows that when the converter is operating under mode-4 it achieves the minimum losses while maximum losses occur in mode-5, thus reinforcing the proposed optimal modes to be used for

Fig. 11. Transformer losses in best and worst modes with Input Voltage $V_1 = 230V$, Output Voltage $V_2^{ref} = 138V$, Conversion ratio d=0.6 and switching frequency f=20kHz..

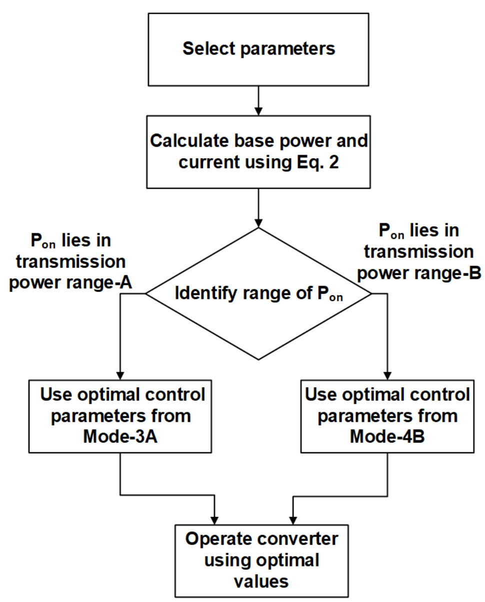

Fig. 12. Flow diagram presenting optimal modulation scheme to minimize transformer losses

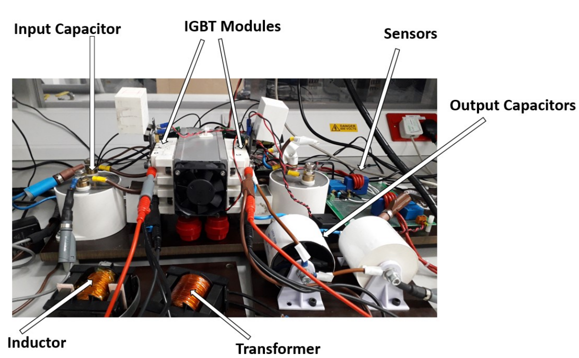

Fig. 13. Experimental setup

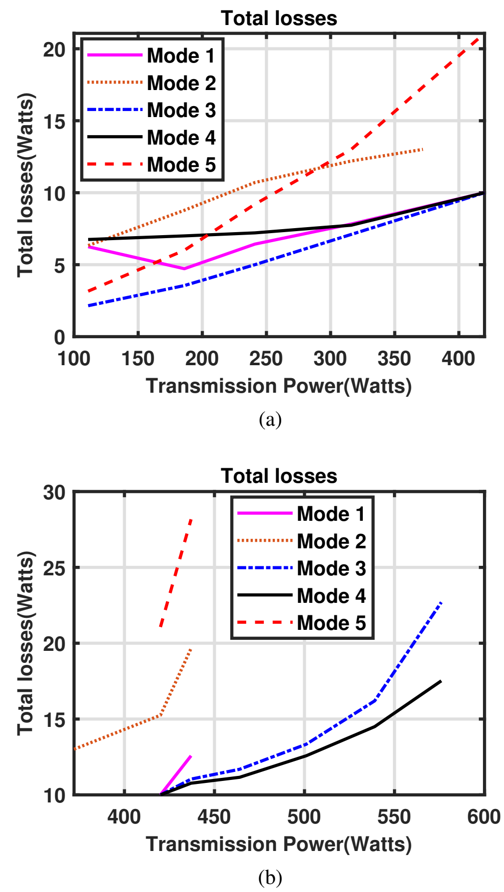

Fig. 14. Total losses of transformer in experimental isolated bidirectional DAB converter with Input Voltage $V_1 = 230V$, Output Voltage $V_2^{ref} = 138V$, Conversion ratio d=0.6 and switching frequency f=20kHz. .(a) Power transmission range-A. (b) Power transmission range-B

Fig. 15. Transformer losses in best and Worst modes(Experimental) with Input Voltage $V_1 = 230V$, Output Voltage $V_2^{ref} = 138V$, Conversion ratio d=0.6 and switching frequency f=20kHz.

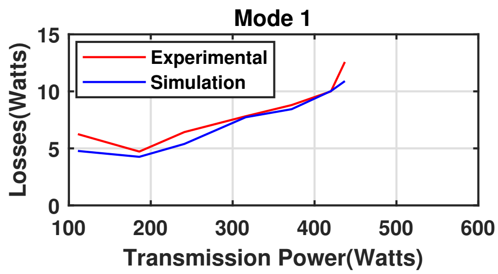

(a)

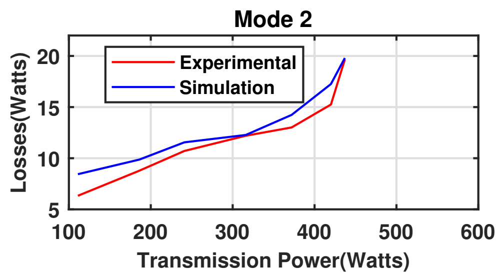

(b)

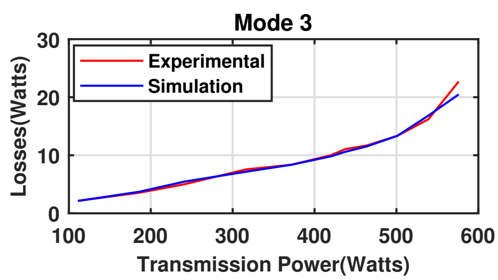

(c)

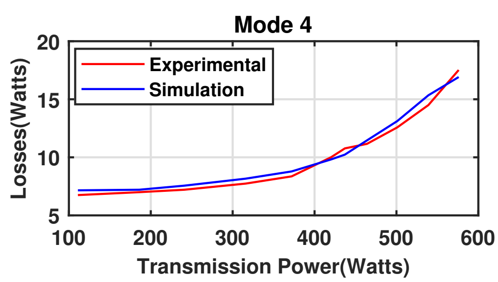

(d)

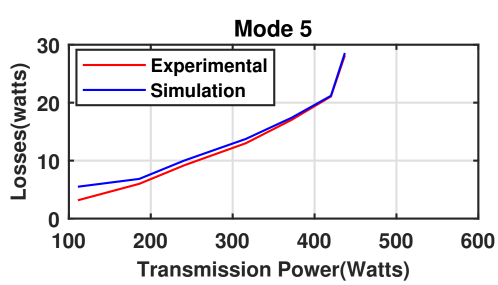

(e)

Fig. 16. Comparison of simulation and experimental results (a) Mode-1 (b) Mode-2 (c) Mode-3 (d) Mode-4 (e) Mode-5

TABLE VI
HARDWARE COMPONENTS

Component	Description	Parameters
Switching devices	SKM75GB176D	$V_{CES} = 1700V$ $I_C = 80A$
Input Capacitors	C4DE	480 μF
Output Capacitors	IEC 61071 DownCap DTR	100 μ F 50 μ F
Magnetic components	Core ETD 59/31/22 N97 Litz Wire	$L_S = 226.6\mu$ H
Voltage sensors	LV 25-p	$t_r = 25\mu$S
Current sensors	LA 55-p	BW=25 μS 200kHz

minimizing the transformer losses. Similarly, Fig. 15 provides a comparison of operating modes resulting in minimum and maximum losses as previously discussed in Section-IV.

The comparisons of the simulation and experimental results for each mode of operation are provided in Fig.16(a-e).

VI. Efficiency of DAB Converter under TPS

The losses in the converter mainly consist of losses occurring in switching devices and the losses in the transformer and inductor. The losses in switching devices can be further categorized as the switching losses and conduction losses [8].

The switching losses depend and can be controlled by applying modulation strategies that result in soft switching. The SPS modulation provides soft switching when conversion ratio is nearly equal to unity, however, it loses soft switching at larger voltage variations in the output. Conversely, TPS provides soft switching at an extended range of operation [6], [7] and [9]–[12]. For the TPS modulation used in this research work to consider the transformer losses, adapted from [7], has been analyzed and proven to be providing soft switching in [7].

The conduction losses in the switching devices depend on the current flowing in the converter and can be minimized by selecting a modulation scheme that results in minimum ac current through the inductor. For the discussed modulation scheme, it is shown in [7] as well as in this research that mode-3 and mode-4 have lowest current. The current waveforms are provided both using simulations Fig. 7 as well as experiment in Fig. 17 for converter operating at P_o=241 watts, input Voltage $V_1 = 230V$, output Voltage $V_2^{ref} = 138V$ and conversion ratio d=0.6. The analysis data of the current waveforms and the resultant losses are provided in Table V. It is apparent from the waveforms that mode-3 has lowest current. Similarly, analysis provided in Table V also confirms that the mode-3 results in minimum current thus minimizing conduction losses.

The other main part of the losses which is the focus of this research are the losses consumed in the transformer and inductor in the form of core losses and winding losses. These losses depend on the current stress as well as the harmonic content of the current waveform as proved in this research. This research has shown that mode-3 and mode-4 have minimum losses for low power and high power ranges, respectively.

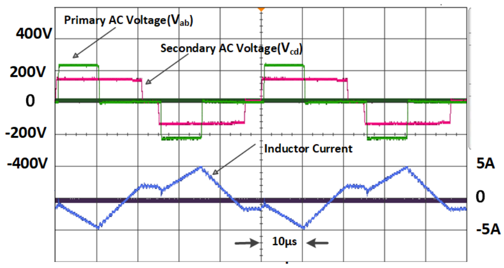

(a)

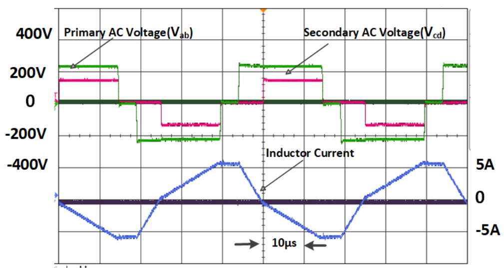

(b)

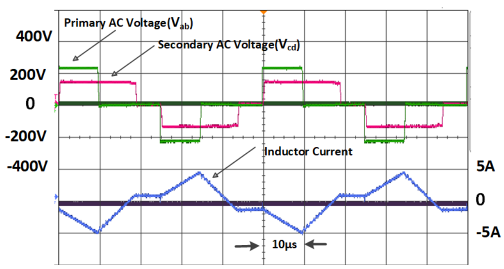

(c)

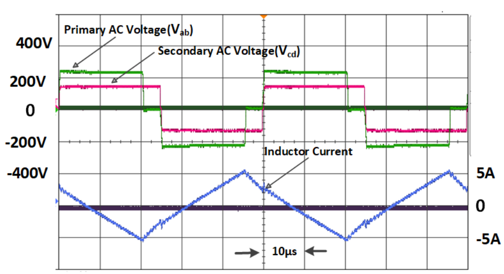

(d)

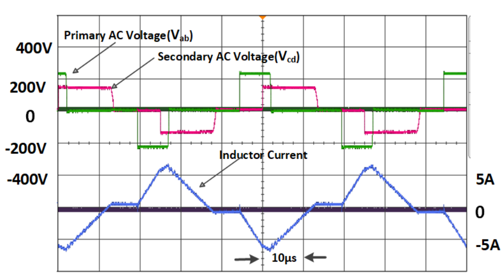

(e)

Fig. 17. Waveforms obtained from laboratory prototype of DAB dc-dc converter operating at P_o=241 watts, Input Voltage $V_1 = 230V$, Output Voltage $V_2^{ref} = 138V$, Conversion ratio d=0.6 and switching frequency f=20kHz. (a) Mode-1 (b) Mode-2 (c) Mode-3 (d) Mode-4 (e) Mode-5

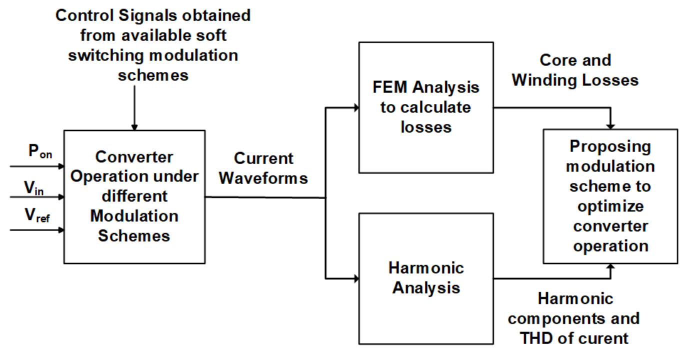

Fig. 18. Generalized framework to optimize transformer losses in isolated converters

VII. Proposed Generalized Framework for Optimisation of Transformer Losses in Isolated Converters

In this section, a generalized framework is proposed to optimize the operation of isolated converters by selecting the optimal modulation scheme which minimizes transformer losses. The block diagram given in Fig. 18 presents the proposed methodology to optimize the converter losses. As switching losses are the main losses occurring in the converter [8], the operating ranges that satisfy the soft switching criterion are generally selected [6]-[7] and [9]–[12]. In order to determine the optimal modulation scheme, the transformer losses must also be calculated and analyzed for different soft switching modulation schemes. FEM analysis can be used to calculate the transformer losses. To conduct FEA, the transformer used in the converter circuit can be modelled using any FEM software, such as ANSYS Maxwell, with the same core shape, material type and winding conditions as used in the design of the converter circuit. To analyze the losses under each operating mode, current waveforms are provided as input to the FEM model of the transformer. The converter needs to be operated under all available modulation scheme with the same parameters for all the schemes to generate the required current waveforms. The current waveforms can be obtained by simulating the converter in PLECS, MATLAB, ANSYS Simplorer or any other suitable software and noting the input and output currents of the magnetic components. The current obtained using the experimental setup of the converter can also be used as the excitation input of the transformer.

Core and winding losses are then calculated using FEA while a harmonic analysis is performed to determine the THD and harmonic components of the current as shown in the two blocks in Fig.18. The applied current waveforms are sufficient to calculate the core loss in the transformer as magnetizing current, which is the difference of the primary and secondary current, can be used to calculate the core losses of the transformer in FEM setup [72] and [73]. The harmonic analysis of the ac current helps to understand and analyze the behaviour of the transformer in that specific converter. It is suggested that the transformer losses are analyzed at different power levels over the available range to obtain an accurate result. This data can be analyzed to select the optimal modulation scheme that minimizes transformer losses in the isolated converter.

VIII. Conclusion

The efficiency of power converters is a research area of high significance. In isolated converters, including the DAB dc-dc converter, transformer losses are one of the factors that contribute to reduced efficiency. The existing literature focuses on the transformer design to minimize losses. In this paper, it is shown that FEM can be used to analyze transformer losses for different operating conditions, and the results used to optimize converter operation. FEA is performed to investigate the impact of the applied modulation scheme on the transformer losses of a DAB dc-dc converter. The current waveforms and the resultant losses for every mode of UTPS modulation at the same transmission power are obtained. The analysis shows that each of the five operating modes of UTPS modulation provides the transformer with an excitation current having a distinct peak and harmonic content, and thus results in different transformer losses for the same required transmission power. Based on this extensive analysis, an optimal modulation scheme for minimum transformer losses has been proposed. Experiments carried out on DAB dc-dc converter prototype confirm the findings. A novel approach to minimize losses in DAB dc-dc converter that could also be extended to other isolated power converters in future work is also presented.

References

[1] R. De Doncker, D. Divan, and M. Kheraluwala, "A three-phase soft-switched high-power-density dc/dc converter for high-power applications," *IEEE Transactions on Industry Applications*, vol. 27, no. 1, pp. 63–73, 1991. DOI: 10.1109/28.67533.

[2] L. G. N. G. Hingorani, *Understanding FACTs: Concept and Technology of Flexible AC Transmission Systems*. Piscataway, NJ, USA: IEEE Press, 2000.

[3] Z. Chen, J. M. Guerrero, and F. Blaabjerg, "A review of the state of the art of power electronics for wind turbines," *IEEE Transactions on Power Electronics*, vol. 24, no. 8, pp. 1859–1875, 2009. DOI: 10.1109/TPEL.2009.2017082.

[4] J. Carrasco, L. Franquelo, J. Bialasiewicz, *et al.*, "Power-electronic systems for the grid integration of renewable energy sources: A survey," *IEEE Transactions on Industrial Electronics*, vol. 53, no. 4, pp. 1002–1016, 2006. DOI: 10.1109/TIE.2006.878356.

[5] S. Bifaretti, P. Zanchetta, A. Watson, L. Tarisciotti, and J. C. Clare, "Advanced power electronic conversion and control system for universal and flexible power management," *IEEE Transactions on Smart Grid*, vol. 2, no. 2, pp. 231–243, 2011. DOI: 10.1109/TSG.2011.2115260.

[6] B. Zhao, Q. Song, W. Liu, and Y. Sun, "Overview of dual-active-bridge isolated bidirectional dc–dc converter for high-frequency-link power-conversion system," *IEEE Transactions on Power Electronics*, vol. 29, no. 8, pp. 4091–4106, 2014. DOI: 10.1109/TPEL.2013.2289913.

[7] J. Huang, Y. Wang, Z. Li, and W. Lei, "Unified triple-phase-shift control to minimize current stress and achieve full soft-switching of isolated bidirectional dc–dc converter," *IEEE Transactions on Industrial Electronics*, vol. 63, no. 7, pp. 4169–4179, 2016. DOI: 10.1109/TIE.2016.2543182.

[8] F. Krismer and J. W. Kolar, "Accurate power loss model derivation of a high-current dual active bridge converter for an automotive application," *IEEE Transactions on Industrial Electronics*, vol. 57, no. 3, pp. 881–891, 2010. DOI: 10.1109/TIE.2009.2025284.

[9] J. Everts, "Closed-form solution for efficient zvs modulation of dab converters," *IEEE Transactions on Power Electronics*, vol. 32, no. 10, pp. 7561–7576, 2017. DOI: 10.1109/TPEL.2016.2633507.

[10] J. Everts, F. Krismer, J. Van den Keybus, J. Driesen, and J. W. Kolar, "Optimal zvs modulation of single-phase single-stage bidirectional dab ac–dc converters," *IEEE Transactions on Power Electronics*, vol. 29, no. 8, pp. 3954–3970, 2014. DOI: 10.1109/TPEL.2013.2292026.

[11] A. Tong, L. Hang, and G. Li, "Optimized control strategy for minimum ohmic loss of dual acitve bridge converter," in *2017 IEEE Applied Power Electronics Conference and Exposition (APEC)*, 2017, pp. 1103–1110. DOI: 10.1109/APEC.2017.7930833.

[12] F. Krismer and J. W. Kolar, "Closed form solution for minimum conduction loss modulation of dab converters," *IEEE Transactions on Power Electronics*, vol. 27, no. 1, pp. 174–188, 2012. DOI: 10.1109/TPEL.2011.2157976.

[13] J. Smajic, J. Hughes, T. Steinmetz, D. Pusch, W. Monig, and M. Carlen, "Numerical computation of ohmic and eddy-current winding losses of converter transformers including higher harmonics of load current," *IEEE Transactions on Magnetics*, vol. 48, no. 2, pp. 827–830, 2012. DOI: 10.1109/TMAG.2011.2171926.

[14] K. D. Hoang and J. Wang, "Design optimization of high frequency transformer for dual active bridge dc-dc converter," in *2012 XXth International Conference on Electrical Machines*, 2012, pp. 2311–2317. DOI: 10.1109/ICElMach.2012.6350205.

[15] J. Liu, L. Sheng, J. Shi, Z. Zhang, and X. He, "Design of high voltage, high power and high frequency transformer in lcc resonant converter," in *2009 Twenty-Fourth Annual IEEE Applied Power Electronics Conference and Exposition*, 2009, pp. 1034–1038. DOI: 10.1109/APEC.2009.4802790.

[16] Y. Lee, G. Vakil, A. J. Watson, and P. W. Wheeler, "Geometry optimization and characterization of three-phase medium frequency transformer for 10kva isolated dc-dc converter," in *2017 IEEE Energy Conversion*

Congress and Exposition (ECCE), 2017, pp. 511–518. DOI: 10.1109/ECCE.2017.8095826.

[17] B. Zhao, Z. Ouyang, M. C. Duffy, M. A. E. Andersen, and W. G. Hurley, "An improved partially interleaved transformer structure for high-voltage high-frequency multiple-output applications," *IEEE Transactions on Industrial Electronics*, vol. 66, no. 4, pp. 2691–2702, 2019. DOI: 10.1109/TIE.2018.2840499.

[18] L. Di Noia, R. Rizzo, R. Miceli, and L. Piegari, "Improving high frequency transformers behavior for dc-dc converter used in electric vehicles," in *2018 7th International Conference on Renewable Energy Research and Applications (ICRERA)*, 2018, pp. 1508–1513. DOI: 10.1109/ICRERA.2018.8567012.

[19] M. Mogorovic and D. Dujic, "100 kw, 10 khz medium-frequency transformer design optimization and experimental verification," *IEEE Transactions on Power Electronics*, vol. 34, no. 2, pp. 1696–1708, 2019. DOI: 10.1109/TPEL.2018.2835564.

[20] M. Leibl, G. Ortiz, and J. W. Kolar, "Design and experimental analysis of a medium-frequency transformer for solid-state transformer applications," *IEEE Journal of Emerging and Selected Topics in Power Electronics*, vol. 5, no. 1, pp. 110–123, 2017. DOI: 10.1109/JESTPE.2016.2623679.

[21] J. Saha, D. Hazarika, N. B. Y. Gorla, and S. K. Panda, "Machine-learning-aided optimization framework for design of medium-voltage grid-connected solid-state transformers," *IEEE Journal of Emerging and Selected Topics in Power Electronics*, vol. 9, no. 6, pp. 6886–6900, 2021. DOI: 10.1109/JESTPE.2021.3074408.

[22] J. Saha, N. B. Y. Gorla, A. Subramaniam, and S. K. Panda, "Computational feasibility of multi-objective optimal design techniques for grid-connected multi-cell solid-state-transformers," in *IECON 2021 – 47th Annual Conference of the IEEE Industrial Electronics Society*, 2021, pp. 1–6. DOI: 10.1109/IECON48115.2021.9589779.

[23] T. Guillod and J. W. Kolar, "Medium-frequency transformer scaling laws: Derivation, verification, and critical analysis," *CPSS Transactions on Power Electronics and Applications*, vol. 5, no. 1, pp. 18–33, 2020. DOI: 10.24295/CPSSTPEA.2020.00003.

[24] P. Czyz, T. Guillod, F. Krismer, J. Huber, and J. W. Kolar, "Design and experimental analysis of 166 kw medium-voltage medium-frequency air-core transformer for 1:1-dcx applications," *IEEE Journal of Emerging and Selected Topics in Power Electronics*, pp. 1–1, 2021. DOI: 10.1109/JESTPE.2021.3060506.

[25] S. Baek and S. Bhattacharya, "Isolation transformer for 3-port 3-phase dual-active bridge converters in medium voltage level," *IEEE Access*, vol. 7, pp. 19 678–19 687, 2019. DOI: 10.1109/ACCESS.2019.2895818.

[26] D. Neumayr, M. Vöhringer, N. Chrysogelos, G. Deboy, and J. W. Kolar, "P^3dct—partial-power pre-regulated dc transformer," *IEEE Transactions on Power Electronics*, vol. 34, no. 7, pp. 6036–6047, 2019. DOI: 10.1109/TPEL.2018.2879064.

[27] J. Saha, N. B. Y. Gorla, A. Subramaniam, and S. K. Panda, "Analysis of modulation and optimal design methodology for half-bridge matrix-based dual-active-bridge (mb-dab) ac-dc converter," *IEEE Journal of Emerging and Selected Topics in Power Electronics*, pp. 1–1, 2021. DOI: 10.1109/JESTPE.2021.3107500.

[28] R. M. Burkart and J. W. Kolar, "Comparative η– ρ–σ pareto optimization of si and sic multilevel dual-active-bridge topologies with wide input voltage range," *IEEE Transactions on Power Electronics*, vol. 32, no. 7, pp. 5258–5270, 2017. DOI: 10.1109/TPEL.2016.2614139.

[29] J. Saha, N. B. Y. Gorla, and S. K. Panda, "Analytical expression-based modulation for soft-switched matrix-based dual-active-bridge (s2mb-dab) single-phase ac-dc converter," *IEEE Journal of Emerging and Selected Topics in Power Electronics*, pp. 1–1, 2021. DOI: 10.1109/JESTPE.2021.3135630.

[30] B. Zhao, Q. Song, and W. Liu, "Efficiency characterization and optimization of isolated bidirectional dc–dc converter based on dual-phase-shift control for dc distribution application," *IEEE Transactions on Power Electronics*, vol. 28, no. 4, pp. 1711–1727, 2013. DOI: 10.1109/TPEL.2012.2210563.

[31] N. Dai and F. Lee, "Edge effect analysis in a high-frequency transformer," in *Proceedings of 1994 Power Electronics Specialist Conference - PESC'94*, vol. 2, 1994, 850–855 vol.2. DOI: 10.1109/PESC.1994.373778.

[32] G. S. Dimitrakakis and E. C. Tatakis, "High-frequency copper losses in magnetic components with layered windings," *IEEE Transactions on Magnetics*, vol. 45, no. 8, pp. 3187–3199, 2009. DOI: 10.1109/TMAG.2009.2018624.

[33] F. Dong Tan, J. Vollin, and S. Cuk, "A practical approach for magnetic core-loss characterization," *IEEE Transactions on Power Electronics*, vol. 10, no. 2, pp. 124–130, 1995. DOI: 10.1109/63.372597.

[34] J. K. Watson, *Applicat. Magnetism*. New York: John Wiley, 1980.

[35] R. M. Bozorth, *Ferromagnetism*. New York: Wiley IEEE Press, 1978.

[36] E. C. Snelling, *Soft Ferrites: Properties and Application, Second Ed.* England: Butterworths, 1988.

[37] S. Sadati, A. Tahani, M. Jafari, and M. Dargahi, "Derating of transformers under non-sinusoidal loads," in *2008 11th International Conference on Optimization of Electrical and Electronic Equipment*, 2008, pp. 263–268. DOI: 10.1109/OPTIM.2008.4602376.

[38] I. Villar, U. Viscarret, I. Etxeberria-Otadui, and A. Rufer, "Global loss evaluation methods for nonsinusoidally fed medium-frequency power transformers," *IEEE Transactions on Industrial Electronics*, vol. 56, no. 10, pp. 4132–4140, 2009. DOI: 10.1109/TIE.2009.2021174.

[39] S. Butterworth, "The high-frequency copper losses in inductance coils," *Experimental Wireless and the Wireless Engineer*, vol. 2, no. 22, pp. 613–616, 2009.

[40] X. Nan and C. Sullivan, “An improved calculation of proximity-effect loss in high-frequency windings of round conductors,” in *IEEE 34th Annual Conference on Power Electronics Specialist, 2003. PESC ’03.*, vol. 2, 2003, 853–860 vol.2. DOI: 10 . 1109 / PESC . 2003 . 1218168.

[41] M. A. Bahmani and et al, “Core loss behavior in high frequency high power transformers—i: Effect of core topology,” *Journal of Renewable and Sustainable Energy*, vol. 4, no. 3, 2012.

[42] C. Steinmetz, “On the law of hysteresis,” *Proceedings of the IEEE*, vol. 72, no. 2, pp. 197–221, 1984. DOI: 10.1109/PROC.1984.12842.

[43] *HF-core losses for non-sinusoidal waveforms,* pp. 140-148: in Proceedings of HFPC, 1991.

[44] J. Reinert, A. Brockmeyer, and R. De Doncker, “Calculation of losses in ferro- and ferrimagnetic materials based on the modified steinmetz equation,” *IEEE Transactions on Industry Applications*, vol. 37, no. 4, pp. 1055–1061, 2001. DOI: 10.1109/28.936396.

[45] J. Li, T. Abdallah, and C. Sullivan, “Improved calculation of core loss with nonsinusoidal waveforms,” in *Conference Record of the 2001 IEEE Industry Applications Conference. 36th IAS Annual Meeting (Cat. No.01CH37248)*, vol. 4, 2001, 2203–2210 vol.4. DOI: 10.1109/IAS.2001.955931.

[46] K. Venkatachalam, C. Sullivan, T. Abdallah, and H. Tacca, “Accurate prediction of ferrite core loss with nonsinusoidal waveforms using only steinmetz parameters,” in *2002 IEEE Workshop on Computers in Power Electronics, 2002. Proceedings.*, 2002, pp. 36–41. DOI: 10.1109/CIPE.2002.1196712.

[47] A. Van den Bossche, V. Valchev, and G. Georgiev, “Measurement and loss model of ferrites with non-sinusoidal waveforms,” in *2004 IEEE 35th Annual Power Electronics Specialists Conference (IEEE Cat. No.04CH37551)*, vol. 6, 2004, 4814–4818 Vol.6. DOI: 10.1109/PESC.2004.1354851.

[48] D. Lin, P. Zhou, W. Fu, Z. Badics, and Z. Cendes, “A dynamic core loss model for soft ferromagnetic and power ferrite materials in transient finite element analysis,” *IEEE Transactions on Magnetics*, vol. 40, no. 2, pp. 1318–1321, 2004. DOI: 10 . 1109 / TMAG . 2004.825025.

[49] E. Bennett and S. C. Larson, “Effective resistance to alternating currents of multilayer windings,” *Electrical Engineering*, vol. 59, no. 12, pp. 1010–1016, 1940. DOI: 10.1109/EE.1940.6435274.

[50] P. Dowell, “Effects of eddy currents in transformer windings,” *Proc. Inst. Electr. Eng*, vol. 113, pp. 1387–1394, 1966. DOI: 10.1049/piee.1966.0236.

[51] J. Ferreira, “Appropriate modelling of conductive losses in the design of magnetic components,” in *21st Annual IEEE Conference on Power Electronics Specialists*, 1990, pp. 780–785. DOI: 10.1109/PESC.1990.131268.

[52] M. B. et al, “Modelling winding losses in high-frequency power inductors,” *J. Circuits, Syst. Comput*, vol. 5, no. 4, pp. 607–626, 1995.

[53] A. Reatti and M. Kazimierczuk, “Comparison of various methods for calculating the ac resistance of inductors,” *IEEE Transactions on Magnetics*, vol. 38, no. 3, pp. 1512–1518, 2002. DOI: 10.1109/20.999124.

[54] F. Robert, P. Mathys, and J.-P. Schauwers, “Ohmic losses calculation in smps transformers: Numerical study of dowell’s approach accuracy,” *IEEE Transactions on Magnetics*, vol. 34, no. 4, pp. 1255–1257, 1998. DOI: 10.1109/20.706513.

[55] A. Lotfi and F. Lee, “Two dimensional field solutions for high frequency transformer windings,” in *Proceedings of IEEE Power Electronics Specialist Conference - PESC ’93*, 1993, pp. 1098–1104. DOI: 10.1109/PESC. 1993.472055.

[56] A. Loth and F. Lee, “Two-dimensional skin effect in power foils for high-frequency applications,” *IEEE Transactions on Magnetics*, vol. 31, no. 2, pp. 1003–1006, 1995. DOI: 10.1109/20.364775.

[57] B. Chen and L. Li, “Semi-empirical model for precise analysis of copper losses in high-frequency transformers,” *IEEE Access*, vol. 6, pp. 3655–3667, 2018. DOI: 10.1109/ACCESS.2018.2797359.

[58] F. Robert, P. Mathys, and J.-P. Schauwers, “A closed-form formula for 2d ohmic losses calculation in smps transformer foils,” in *APEC ’99. Fourteenth Annual Applied Power Electronics Conference and Exposition. 1999 Conference Proceedings (Cat. No.99CH36285)*, vol. 1, 1999, 199–205 vol.1. DOI: 10.1109/APEC.1999. 749510.

[59] ——, “A closed-form formula for 2-d ohmic losses calculation in smps transformer foils,” *IEEE Transactions on Power Electronics*, vol. 16, no. 3, pp. 437–444, 2001. DOI: 10.1109/63.923777.

[60] B. W. R. Kasikowski, “Ascertainment of fringing-effect losses in ferrite inductors with an air gap by thermal compact modelling and thermographic measurements,” *Applied Thermal Engineering*, vol. 124, no. 4, pp. 1447–1456, 2017.

[61] A.-T. Phung, G. Meunier, O. Chadebec, X. Margueron, and J.-P. Keradec, “High-frequency proximity losses determination for rectangular cross-section conductors,” *IEEE Transactions on Magnetics*, vol. 43, no. 4, pp. 1213–1216, 2007. DOI: 10 . 1109 / TMAG . 2007 . 892303.

[62] F. Robert, P. Mathys, B. Velaerts, and J.-P. Schauwers, “Two-dimensional analysis of the edge effect field and losses in high-frequency transformer foils,” *IEEE Transactions on Magnetics*, vol. 41, no. 8, pp. 2377–2383, 2005. DOI: 10.1109/TMAG.2005.852938.

[63] R. P. Wojda and M. K. Kazimierczuk, “Winding resistance and power loss of inductors with litz and solid-round wires,” *IEEE Transactions on Industry Applications*, vol. 54, no. 4, pp. 3548–3557, 2018. DOI: 10. 1109/TIA.2018.2821647.

[64] W. A. Roshen, “Fringing field formulas and winding loss due to an air gap,” *IEEE Transactions on Magnetics*, vol. 43, no. 8, pp. 3387–3394, 2007. DOI: 10.1109/ TMAG.2007.898908.

[65] G. S. Dimitrakakis, E. C. Tatakis, and E. J. Rikos, "A semiempirical model to determine hf copper losses in magnetic components with nonlayered coils," *IEEE Transactions on Power Electronics*, vol. 23, no. 6, pp. 2719–2728, 2008. DOI: 10 . 1109 / TPEL . 2008 . 2004872.

[66] V. Sarac, "Fem 2d and 3d design of transformer for core losses computation," in *(2017) In: XIV International Scientific Congress 13-16 Sept 2017, Varna, Bulgaria*, 2017.

[67] A. Konrad, "Integrodifferential finite element formulation of two-dimensional steady-state skin effect problems," *IEEE Transactions on Magnetics*, vol. 18, no. 1, pp. 284–292, 1982. DOI: 10 . 1109 / TMAG . 1982 . 1061775.

[68] J. Weiss and Z. J. Csendes, "A one-step finite element method for multiconductor skin effect problems," *IEEE Transactions on Power Apparatus and Systems*, vol. PAS-101, no. 10, pp. 3796–3803, 1982. DOI: 10.1109/TPAS.1982.317065.

[69] A. Konrad, M. Chari, and Z. Csendes, "New finite element techniques for skin effect problems," *IEEE Transactions on Magnetics*, vol. 18, no. 2, pp. 450–455, 1982. DOI: 10.1109/TMAG.1982.1061859.

[70] https://www.ansys.com/.

[71] https://www.plexim.com/products/plecs.

[72] S. Magdaleno-Adame, T. D. Kefalas, S. Garcia-Martinez, and C. Perez-Rojas, "Electromagnetic finite element analysis of electrical steels combinations in lamination core steps of single-phase distribution transformers," in *2017 IEEE International Autumn Meeting on Power, Electronics and Computing (ROPEC)*, 2017, pp. 1–5. DOI: 10.1109/ROPEC.2017.8261585.

[73] T. D. Kefalas and S. Magdaleno-Adame, "Fe-based application for the evaluation of core-losses in distribution transformers," in *2018 XIII International Conference on Electrical Machines (ICEM)*, 2018, pp. 2393–2399. DOI: 10.1109/ICELMACH.2018.8507043.

Seema Akbar received master's in electrical engineering from National University of Sciences and Technology, Islamabad, Pakistan in 2016. Currently, she is pursuing her PhD degree in electrical engineering from the National University of Sciences and Technology, Islamabad, Pakistan. She was a visiting research scholar with Power Electronics Machines and Control Group, University of Nottingham from October 2019 to October 2021. Her current research interests include model predictive control and optimization of power electronic converters.

Ammar Hasan was born in Pakistan in 1982. He received the B.E. degree in electrical engineering from the National University of Sciences and Technology, Islamabad, Pakistan, in 2004, and the master's and PhD degrees in control systems from the Imperial College London, London, U.K., in 2008 and 2012, respectively.

Since 2012, he has been with the School of Electrical Engineering and Computer Science, National University of Sciences and Technology, where he is currently an Associate Professor. His current research interests include model predictive control, control of power electronic converters, optimization techniques for control systems, and numerical algorithms as dynamical systems.

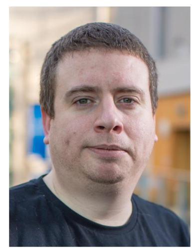

Alan Watson (S'03–M'08-SM'21) received an M.Eng. (Hons.) degree in Electronic Engineering from the University of Nottingham, UK in 2004, and a PhD, also from the University of Nottingham in 2008. In 2009, he became a Research Fellow with the Power Electronics Machines and Control Group, University of Nottingham. Since 2009, he has been involved in various projects in the area of high-power electronics including resonant converters, high voltage power supplies, and multilevel converters for grid connected applications such as HVDC and Flexible AC Transmission Systems. In 2012, he was promoted to Senior Research Fellow before becoming an Assistant Professor in High Power Electronics at the University of Nottingham in 2013. His current research interests include the development and control of advanced high-power conversion topologies for industrial applications, grid connected converters and HVDC Transmission.

Prof. Pat Wheeler received his BEng [Hons] degree in 1990 from the University of Bristol, UK. He received his PhD degree in Electrical Engineering for his work on Matrix Converters from the University of Bristol, UK in 1994. In 1993 he moved to the University of Nottingham and worked as a research assistant in the Department of Electrical and Electronic Engineering. In 1996 he became a Lecturer in the Power Electronics, Machines and Control Group at the University of Nottingham, UK. Since January 2008 he has been a Full Professor in the same research group.

He was Head of the Department of Electrical and Electronic Engineering at the University of Nottingham from 2015 to 2018. He is currently the Head of the Power Electronics, Machines and Control Research Group, Global Director of the University of Nottingham's Institute of Aerosapce Technology and was the Li Dak Sum Chair Professor in Electrical and Aerospace Engineering. He is a member of the IEEE PELs AdCom and is currently IEEE PELS Vice-President for Technical Operations. He has published over 750 academic publications in leading international conferences and journals.